Macroscopic Transport of Mega-ampere Electron Currents in Aligned Carbon-Nanotube Arrays

Gourab Chatterjee,[1] Prashant Kumar Singh,[1] Saima Ahmed,[1] A. P. L. Robinson,[2] Amit D. Lad,[1] Sudipta Mondal,[1] V. Narayanan,[1] Iti Srivastava,[3] Nikhil Koratkar,[4,3] John Pasley,[5,2] A. K. Sood,[6] and G. Ravindra Kumar[1,*]

[1]*Tata Institute of Fundamental Research, Homi Bhabha Road, Mumbai, 400005, India*
[2]*Central Laser Facility, Rutherford-Appleton Laboratory, Chilton, Didcot, OX10 0QX, United Kingdom*
[3]*Department of Materials Science and Engineering, Rensselaer Polytechnic Institute, Troy, New York 12180, USA*
[4]*Department of Mechanical, Aerospace and Nuclear Engineering, Rensselaer Polytechnic Institute, Troy, New York 12180, USA*
[5]*York Plasma Institute, University of York, Heslington, York, YO10 5DQ, United Kingdom*
[6]*Department of Physics, Indian Institute of Science, Bangalore, 560 012, India*

(Received 28 January 2012; published 8 June 2012)

We demonstrate that aligned carbon-nanotube arrays are efficient transporters of laser-generated mega-ampere electron currents over distances as large as a millimeter. A direct polarimetric measurement of the temporal and the spatial evolution of the megagauss magnetic fields (as high as 120 MG) at the target rear at an intensity of $(10^{18}$–$10^{19})$ W/cm^2 was corroborated by the rear-side hot electron spectra. Simulations show that such high magnetic flux densities can only be generated by a very well collimated fast electron bunch.

DOI: 10.1103/PhysRevLett.108.235005 PACS numbers: 52.25.Fi, 52.38.Hb, 52.65.Rr

Intense, relativistic ultrashort electron pulses are generated when an ultraintense, femtosecond laser explosively ionizes matter. These electron pulses, constituting mega-ampere currents, are extremely important for high-energy-density science [1], laboratory astrophysics [2], fast ignition of laser fusion [3], novel particle acceleration technologies [4], and ultrafast x-ray sources [5,6]. For instance, in the fast ignition scheme of laser fusion, such mega-ampere electron currents are required to initiate the fusion spark in a precompressed fuel pellet [7]. However, the transport of relativistic electrons through the very medium of their origin—namely, the dense, hot plasma—is fraught with the well-known filamentary (Weibel) instability [8]. This instability, arising from the electromagnetic interaction of the relativistic forward current with the nullifying return current generated by the background plasma, retards and breaks up the forward current into microscopic filaments, destroying beam integrity and limiting beam transport to a few tens of microns [9–11]. Such filamentation is detrimental to all the aforesaid applications, and serious efforts are being made to understand and improve the collimation of these mega-ampere electron currents [12–15]. It is therefore very important to find experimental conditions and target designs where low-divergence transport over long distances can be facilitated.

Simulations [9,10] have predicted in detail the patterns of beam filamentation and the localization of the self-generated magnetic fields, indicative of the extent of penetration of the electron pulses into the medium. In spite of years of investigation through a variety of experimental techniques investigating x-ray, optical, and ion emission from the rear of the target, a direct, quantitative measure of the transport process is still elusive.

In this Letter, we demonstrate the transport of mega-ampere electron pulses over macroscopic (millimeter) distances, 100 times longer than typical filamentation lengths [16]. Such uninhibited electron transport was achieved in specially designed targets, namely self-adhering, self-supporting, aligned carbon-nanotube (CNT) arrays. As a direct and unambiguous measure of the evolution of the hot electron transport, we monitored the self-generated megagauss magnetic fields by optical polarimetry. In addition to the magnitude of the magnetic fields, we capture their subpicosecond-resolved temporal evolution as well as their spatial profile on a micrometer scale. We also present conventional x-ray bremsstrahlung and electron spectrometer (ESM) measurements [17] in support of the magnetic field measurements. Two-dimensional (2D) particle-in-cell (PIC) simulations show that very strong magnetic fields can be produced as the fast electron bunch crosses the target-vacuum interface at the rear surface. In order to produce the multimegagauss magnetic fields that are observed experimentally, the fast electron bunch has to be extremely well collimated; that is, its diameter must be close to the initial laser spot diameter.

Aligned, self-adhering, self-supporting multiwalled CNT arrays (inset of Fig. 1) of mass density 0.264 g/cm^3 were grown by the thermal chemical vapor deposition of ethylene (used as the carbon source) [18,19]. The experiment was performed with the 20 TW Ti:sapphire chirped pulse amplified laser at the Tata Institute of Fundamental Research in Mumbai, operated at a repetition rate of 5 Hz. A p-polarized 40 fs "pump" laser pulse (with a nanosecond contrast of 10^{-6} and peaked around a central wavelength of 800 nm) was focused to a spot size of 17 μm at an oblique incidence of nearly 40° on the target with an $f/3$ off-axis parabolic mirror, creating an intensity

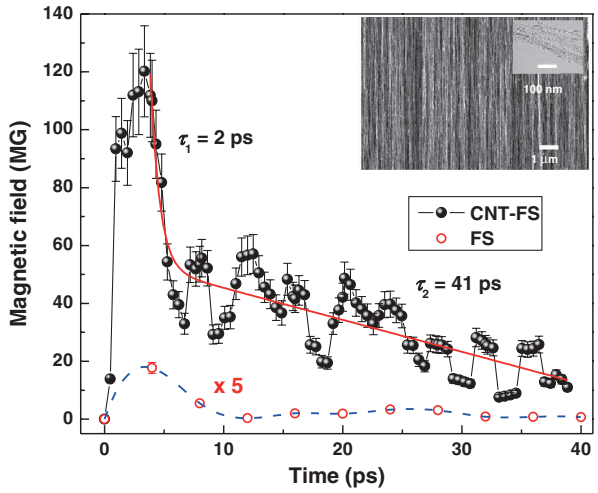

FIG. 1 (color). Temporal evolution of the rear-side magnetic fields for the CNT-FS sandwich target and the FS only target (enhanced five times for comparison) captured at an intensity of (2–4) $\times$ 10^{18} W/cm^2. The different time constants are represented by τ. The inset shows the scanning electron microscope image of the target. The average tube-to-tube spacing between the nanotubes is ~50 nm. The transmission electron microscope image shows that the average diameter of the CNT is ~10 nm.

of (10^{18}–10^{19}) W/cm^2. The temporal and spatial evolution of the megagauss magnetic fields at the target rear were monitored by a time-delayed "probe" pulse (800 nm, 80 fs), generated by extracting a small fraction of the pump pulse. This probe pulse was loosely focused to nearly five times the pump beam diameter to yield a moderate intensity of the order of 10^{11} W/cm^2, thereby encompassing the entire region of the plasma formed by the laser interaction.

The polarimetric measurements of the Stokes parameters of the probe were in accordance with standard procedures [20,21] and have been discussed in detail in our previous work [22–24]. As shown in numerous simulations [9,25], the most significant change was observed in the ellipticity of the polarization state of the incident probe pulse according to the magneto-optic Cotton-Mouton effect due to the predominantly azimuthal geometry of the magnetic fields generated at the target rear [26,27].

The polarimetric technique adopted is crucially dependent on the specular reflection from the target. Nonspecular reflections (i) depolarize the beam, defeating the crucial measurement of the polarization change caused by the magnetic fields (often quite small) and (ii) provide a weak scattered signal, making measurements difficult. The opaque, nonplanar CNT target posed a challenge for measuring the magnetic fields, which was overcome by bonding a thin (100 μm) optically polished fused-silica (FS) "screen" to the rear surface of the 1100-μm thick CNT target with a very thin (a few microns) adhesive layer. As discussed later, the magnetic field measurements indicate that the FS screen is not a significant perturber of the relativistic electron transport in CNT. In addition, hot electron spectrum measurements were made with and without the FS screen and no significant variations were observed due to the presence of the adhesive layer and FS. In regard to the front surface interaction, recent measurements [28] show that the preplasma formation with CNT targets will not be too dissimilar to that observed with a nonstructured-carbon surface.

Figure 1 presents the temporal evolution of the magnetic fields measured at the FS-vacuum interface for both the carbon-nanotube–fused-silica (CNT-FS) sandwich and the plain FS targets. The magnetic pulse has a peak value of 3 MG in the case of FS and lasts essentially for about 10 ps. In contrast, for the CNT-FS target, the magnetic field rises to a peak value of 120 MG, followed by an exponential decay with two distinct temporal components of 2 and 41 ps, respectively. It is worth noting from the peak magnetic fields in Fig. 1 that the FS layer in the sandwich does not appear to significantly retard the fast electron bunch that has traversed the long path in the CNT target. The temporal profile of the magnetic field also shows an oscillatory behavior, which possibly reflects instabilities in the motion of the critical surface and needs to be explored further. Identical measurements with a similar nonstructured-carbon–FS sandwich target could not detect any measurable magnetic field above the noise threshold, as expected.

As shown in Fig. 1, the CNT-FS sandwich target shows a rear-side magnetic field two orders of magnitude larger than that of the FS target even after a transport length that is 10 times larger. This strongly suggests that a high-current-density electron bunch has been very efficiently transported to the rear surface of the CNT-FS target. In order to verify the assumption that strong magnetic fields imply an efficient bunch transport, a set of 2D PIC calculations was performed. These simulations were carried out using the OSIRIS code on a 40 $\times$ 80 μm simulation box containing a 6 $\times$ 70 μm plasma slab of density $20n_c$, where n_c is the critical density. In the central region of this slab, part of the electron population was initialized as a beamlike bunch with an average energy of 1 MeV at an intensity of 5 $\times$ 10^{18} W/cm^2. All other electrons were thermal electrons with a temperature of 2 keV. The bunch had a length equal to the thickness of the slab (6 μm or equivalently a 20 fs pulse duration). The density and the width of the bunch were varied between the simulations. The bunch was then made to propagate into the vacuum region, thereby generating strong magnetic fields in the vacuum and in a thin layer at the plasma surface. An example is shown in Fig. 2. Magnetic flux densities close to the experimentally observed results (for example, the 50 MG magnetic fields in the example shown in Fig. 2) could only be produced if the bunch width and density were close to those expected just after the bunch was produced by the laser interaction (that is, a bunch width of about 16 μm and a bunch density of

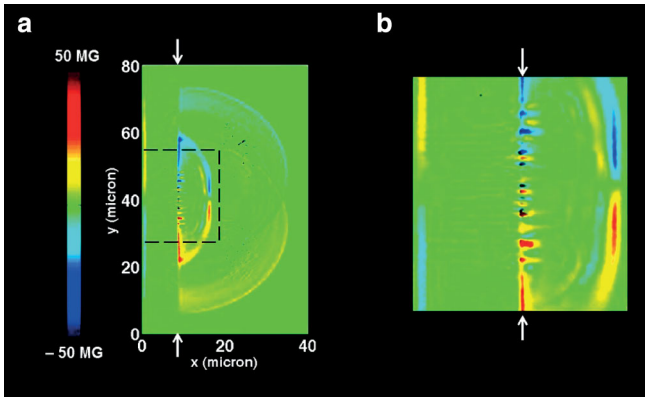

FIG. 2 (color). (a) A snapshot of the B_z component of the magnetic flux density in and around the target from a 2D PIC code simulation using OSIRIS at 88 fs. The arrows indicate the original position of the target-vacuum interface. (b) An enlargement of the boxed region of (a) showing details of the field structure within the target in the region where the electron beam passes through.

about $1n_c$). However, the bunch can only retain this density and width if the transport of the bunch through the CNT array is extremely efficient and prevents any spreading of the bunch. Any bunch spreading increases the width and reduces the density of the fast electron bunch that arrives at the rear surface. The 2D PIC simulations showed that doubling the initial bunch width beyond near-ideal collimation would at least halve the magnetic flux density produced at the rear surface, thereby deviating significantly from the experimentally measured values of the magnetic field. In fact, a recent simulation [29] offers indication of the collimation of mega-ampere electron currents along the surface of CNTs due to a "push-pull" effect generated by the surface electric and magnetic fields. The simulations in Ref. [29] indicate collimation over a length scale of only 12 μm. Our observations show collimated electron transport over a macroscopic distance of 1100 μm.

The spatial profile of the magnetic field in Fig. 3 shows a high level of inhomogeneity and its coalescence demonstrates localization of current, indicative of filamentation [25,30–32]. Most importantly, it shows a large central hollow (negligible magnetic field), which, although predicted in simulations [9,31], has not previously been experimentally observed. The magnetic fields get concentrated in a ringlike pattern inside the plasma due to a "spatial resonance" [31] caused by the radial inhomogeneity in beam density. As shown in Fig. 3, the spatial profile of the magnetic field at the rear of the CNT-FS target is similar to that for FS alone, despite a ten times greater transport length. This is indicative of near-ideal collimated transport in CNT in agreement with the simulations.

The spatial profile of the magnetic fields can be analyzed further by estimating the approximate current density at the target rear. Taking the curl of the measured magnetic fields and considering only the transverse variation, we obtain the current density [Fig. 3(d)] 3 ps after the pump irradiation, which clearly shows the current flow in both the directions, as predicted in simulations [25,30]. Further, the magnitude of the current density reaches local peaks in the range 10^{12} A/cm^2, which is quite substantial and is of the same order as that in the critical surface.

In addition to the magnetic field measurements, we have measured the energy of the hot electrons outside the target

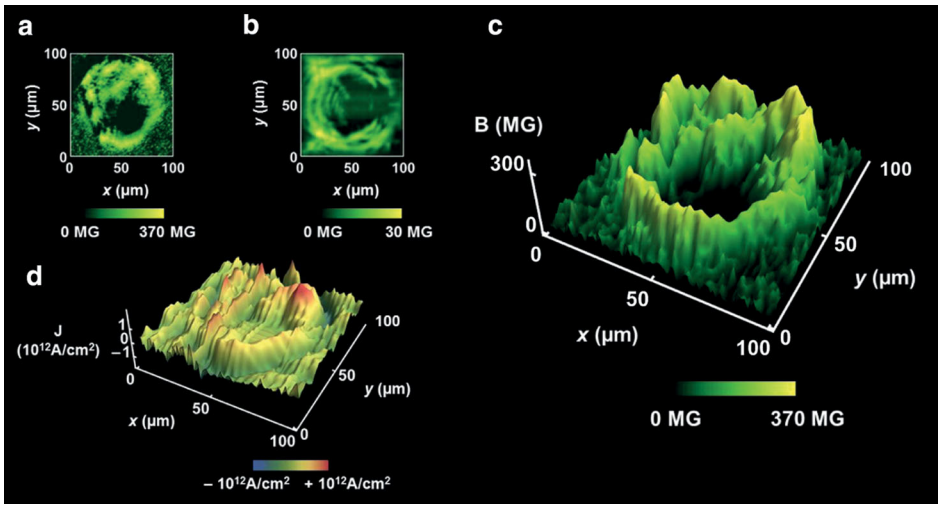

FIG. 3 (color). Two-dimensional spatial profile of the magnetic fields 3 ps after pump irradiation at the rear side of (a) the CNT-FS sandwich target and (b) only FS at an intensity of (2–4) $\times 10^{18}$ W/cm^2. (c) The spatial profile in (a) represented in three dimensions, clearly showing the central hollow and local magnetic field peaks as high as 370 MG, in contrast with only 30 MG for FS alone. (d) Three-dimensional plot of the current density of the CNT-FS sandwich target, derived from the magnetic field spatial profile shown in (a). Note the positive (towards red) and negative (towards blue) current densities.

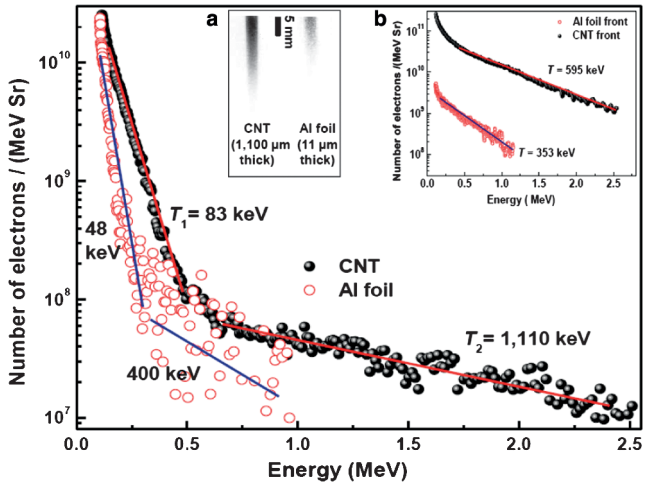

FIG. 4 (color). Energy spectrum of the electrons emitted from the rear side of CNT and Al foil at (4–7) $\times$ 10^{18} W/cm^2 (the Al-foil data are for comparison). The error in the temperature for the CNT target is $\pm$1 keV (83 keV component) and $\pm$30 keV (1110 keV component), and for Al foil $\pm$3 keV (48 keV component) and $\pm$100 keV (400 keV component). (a) Raw traces on the image plate in the ESM. (b) Energy spectrum of the electrons emitted from the front side of aligned CNT at the same intensity. The data were collected over 200 laser shots.

by conventional electron spectrometry. Figure 4 displays the hot electron spectra at the rear of the 1100-μm thick aligned CNT target, which shows hot electron temperatures of 83 keV and 1.1 MeV. This is considerably greater than the 48 keV (and a weak component at 400 keV) for the 11-μm thick Al foil (used for comparison). Inset (a) shows the raw traces of the electron trajectories in the ESM, which unambiguously shows the difference between the darker, longer image of electrons in CNT (indicating a significantly higher electron flux as well as a considerably higher energy of the emitted electrons) and the faint, short one for Al foil. It is important to note the stark contrast between the ESM traces, although the electrons have traveled 100 times longer in CNT (1100 μm), as opposed to only 11 μm in the Al foil. As expected, the measured hot electron spectrum at the rear of the 100-μm thick FS target was found to be relatively weaker, both in terms of flux as well as temperature, compared to the 11-μm thick Al foil, whereas that for the nonstructured-carbon–FS sandwich target was barely detectable (see the Supplemental Material [33]). Thus, even conventional electron spectrometry clearly corroborates the generation and transport of a larger flux of hot electrons through the CNT target, although the electrons are retarded by the sheath field at the target-vacuum interface [34]. Note that the mean free path for these relativistic electrons is larger than the CNT target thickness, making collisional effects insignificant.

Inset (b) in Fig. 4 shows a hot electron temperature of 595 keV at the front of the CNT target, reiterating the role of the CNT nanostructure in enhancing laser absorption and hot electron temperature. In view of the importance of the relativistic electrons generated by the various collective processes in laser plasmas [35], target engineering (particularly nanostructuring of the target surface [36–40], including CNT deposition [28,41]) has been shown to significantly enhance hot electron fluxes and energies due to the additional couplings (for example, the lightning rod effect, surface plasmon excitation, etc.) provided by the nanostructures. Our measurements of x-ray bremsstrahlung emission in the range 150–400 keV at a moderate laser intensity of 2×10^{17} W/cm^2 also support the hot electron spectra at the target front as they yield a hot electron temperature of 60 keV for CNT, as opposed to only 17 keV for a polished metal foil (see the Supplemental Material [33]).

In conclusion, we have demonstrated efficient transport of relativistic electrons over macroscopic distances (1100 μm) in aligned arrays of multiwalled CNTs, significantly larger than the typical filamentation length of a few microns in a solid. In light of the numerous experiments and simulations [42,43] demonstrating the inability of low-density targets to provide adequate return currents to compensate the forward currents, we believe this result will have major implications for understanding the physics of the long-range transport of mega-ampere, relativistic currents, for example, in the fast ignition of laser-fusion and laser-particle acceleration. In general, the transport of large currents of relativistic electrons could open up interesting new questions in high-energy-density science, condensed-matter science, accelerator technologies, and plasma physics.

G. R. K. acknowledges support from a DAE-SRC-ORI grant (DAE, Government of India) and the J. C. Bose grant (DST, Government of India). N. K. acknowledges funding support from the U.S. National Science Foundation (Grant No. 0653589). A. P. L. R. is grateful for the use of computational resources provided by STFC's e-Science facility.

*To whom all correspondence should be addressed.
grk@tifr.res.in

[1] R. P. Drake, *High-Energy-Density Physics* (Springer-Verlag, Berlin, 2006).
[2] B. A. Remington, D. Arnett, R. P. Drake, and H. Takabe, Science **284**, 1488 (1999).
[3] M. Tabak, J. Hammer, M. E. Glinsky, W. L. Kruer, S. C. Wilks, J. Woodworth, E. M. Campbell, M. D. Perry, and R. J. Mason, Phys. Plasmas **1**, 1626 (1994).
[4] E. Esarey, C. B. Schroeder, and W. P. Leemans, Rev. Mod. Phys. **81**, 1229 (2009).
[5] M. M. Murnane, H. C. Kapteyn, M. D. Rosen, and R. W. Falcone, Science **251**, 531 (1991).
[6] B. Dromey *et al.*, Nature Phys. **2**, 456 (2006).
[7] R. Kodama *et al.*, Nature (London) **432**, 1005 (2004).
[8] E. S. Weibel, Phys. Rev. Lett. **2**, 83 (1959).
[9] A. Pukhov, Phys. Rev. Lett. **86**, 3562 (2001).

[10] Y. Sentoku, K. Mima, P. Kaw, and K. Nishikawa, Phys. Rev. Lett. **90**, 155001 (2003).
[11] M. S. Wei *et al.*, Phys. Rev. E **70**, 056412 (2004).
[12] A. R. Bell and R. J. Kingham, Phys. Rev. Lett. **91**, 035003 (2003).
[13] A. P. L. Robinson, M. Sherlock, and P. A. Norreys, Phys. Rev. Lett. **100**, 025002 (2008).
[14] B. Ramakrishna *et al.*, Phys. Rev. Lett. **105**, 135001 (2010).
[15] P. McKenna *et al.*, Phys. Rev. Lett. **106**, 185004 (2011).
[16] L. Gremillet, G. Bonnaud, and F. Amiranoff, Phys. Plasmas **9**, 941 (2002).
[17] K. A. Tanaka, T. Yabuuchi, T. Sato, R. Kodama, Y. Kitagawa, T. Takahashi, T. Ikeda, Y. Honda, and S. Okuda, Rev. Sci. Instrum. **76**, 013507 (2005).
[18] Typically, a 10-nm Al layer and a (1–3)-nm Fe layer were deposited by an electron beam on the surface of a 1-μm thick SiO_2-covered Si wafer in the presence of Ar/H_2 (15% H_2 content) buffer gas. The CNT growth temperature was (750–800) °C. Postsynthesis by chemical vapor deposition, the CNT array was detached from the substrate, as shown in Ref. [19].
[19] Z. Wang, L. Ci, L. Chen, S. Nayak, M. P. Ajayan, and N. Koratkar, Nano Lett. **7**, 697 (2007).
[20] I. H. Hutchinson, *Principles of Plasma Diagnostics* (Cambridge University Press, New York, 1987).
[21] S. E. Segre, Plasma Phys. Controlled Fusion **41**, R57 (1999).
[22] A. S. Sandhu, A. K. Dharmadhikari, P. P. Rajeev, G. R. Kumar, S. Sengupta, A. Das, and P. K. Kaw, Phys. Rev. Lett. **89**, 225002 (2002).
[23] A. S. Sandhu, G. R. Kumar, S. Sengupta, A. Das, and P. K. Kaw, Phys. Rev. E **73**, 036409 (2006).
[24] S. Kahaly, S. Mondal, G. R. Kumar, S. Sengupta, A. Das, and P. K. Kaw, Phys. Plasmas **16**, 043114 (2009).
[25] Y. Sentoku, K. Mima, P. Kaw, and K. Nishikawa, Phys. Rev. E **65**, 046408 (2002).
[26] M. Tatarakis *et al.*, Nature (London) **415**, 280 (2002).
[27] Note that the polarimetric method we employed is independent of the "*X*-wave cutoff method," as pointed out by M. Tatarakis *et al.*, Phys. Plasmas **9**, 2244 (2002). In our experiment, the *X* wave of the externally launched probe has a turning point earlier than the *O* wave in the plasma (the *X*-wave cutoff) and the additional phase difference between the *X* wave and the *O* wave results in an induced ellipticity of the probe, measured in terms of the difference between the refractive indices of the *O* and *X* waves, according to the Appleton-Hartree formula.
[28] S. Bagchi, P. P. Kiran, A. M. Rao, M. K. Bhuyan, M. Krishnamurthy, and G. R. Kumar, Phys. Plasmas **18**, 014502 (2011).
[29] Y. Ji, G. Jiang, W. Wu, C. Wang, Y. Gu, and Y. Tang, Appl. Phys. Lett. **96**, 041504 (2010).
[30] M. Honda, J. Meyer-ter-Vehn, and A. Pukhov, Phys. Plasmas **7**, 1302 (2000).
[31] F. Califano, D. DelSarto, and F. Pegoraro, Phys. Rev. Lett. **96**, 105008 (2006).
[32] C. Ren, M. Tzoufras, F. S. Tsung, W. B. Mori, S. Amorini, R. A. Fonseca, L. O. Silva, J. C. Adam, and A. Heron, Phys. Rev. Lett. **93**, 185004 (2004).
[33] See Supplemental Material at http://link.aps.org/supplemental/10.1103/PhysRevLett.108.235005 for the hot electron spectra at the rear side of the 100-μm thick FS target as well as the nonstructured-carbon–FS sandwich target and for x-ray bremsstrahlung measurements.
[34] T. Yabuuchi *et al.*, Phys. Plasmas **14**, 040706 (2007).
[35] P. Gibbon, *Short Pulse Laser Interactions with Matter: An Introduction* (Imperial College Press, London, 2005).
[36] P. P. Rajeev, P. Taneja, P. Ayyub, A. S. Sandhu, and G. R. Kumar, Phys. Rev. Lett. **90**, 115002 (2003).
[37] S. Kahaly, S. K. Yadav, W. M. Wang, S. Sengupta, Z. M. Sheng, A. Das, P. K. Kaw, and G. R. Kumar, Phys. Rev. Lett. **101**, 145001 (2008).
[38] S. P. Gordon, T. Donnelly, A. Sullivan, H. Hamster, and R. W. Falcone, Opt. Lett. **19**, 484 (1994).
[39] T. Nishikawa, H. Nakano, H. Ahn, N. Uesugi, and T. Serikawa, Appl. Phys. Lett. **70**, 1653 (1997).
[40] G. Kulcsár, D. AlMawlawi, F. W. Budnik, P. R. Herman, M. Moskovits, L. Zhao, and R. S. Majoribanks, Phys. Rev. Lett. **84**, 5149 (2000).
[41] T. Nishikawa, S. Suzuki, Y. Watanabe, O. Zhou, and H. Nakano, Appl. Phys. B **78**, 885 (2004).
[42] D. Batani *et al.*, Phys. Rev. Lett. **94**, 055004 (2005).
[43] Y. T. Li *et al.*, Phys. Rev. E **72**, 066404 (2005).